Journal of Environmental Sciences 168 (2026) 448–455

Contents lists available at ScienceDirect

Journal of Environmental Sciences

journal homepage: www.elsevier.com/locate/jes

JES JOURNAL OF ENVIRONMENTAL SCIENCES www.jesc.ac.cn

Research Article

Investigating the photosensitized chemistry of proxies for tropospheric brown carbon

Jiejing Kong[a,b], Mingzhu He[a], Jintao Liu[a], Xinke Wang[b,c], Sebastien Perrier[b], Taicheng An[a,*], Christian George[b,*]

[a] Guangdong Key Laboratory of Environmental Catalysis and Health Risk Control, School of Environmental Science and Engineering, Institute of Environmental Health and Pollution Control, Guangdong University of Technology, Guangzhou 510006, China
[b] Universite Claude Bernard Lyon 1, CNRS, IRCELYON, UMR 5256, Villeurbanne, F-69100, France
[c] Department of Chemistry, University of Toronto, Toronto, ON M5S 3H6, Canada

ARTICLE INFO

Keywords:
Photosensitized oxidation
Brown carbon (BRC)
Triplet-state chemistry
Organic compounds
Aqueous-phase reactions

ABSTRACT

Brown carbon (BrC) profoundly influences secondary organic aerosol (SOA) formation via photosensitized reactions in atmospheric condensed phases, yet the intrinsic oxidative power of its excited triplet state remains mechanistically unresolved. We reveal that the BrC proxy 1,4-naphthoquinone (NQ) undergoes dual photochemical pathways in deoxygenated aqueous systems, simultaneous self-photoconversion and substrate oxidation, enabled by two distinct, long-lived triplet states (^{3}NQ* and ^{3}OH–NQ*) with $^3(n, \pi^*)$ configurations generated under 355 nm irradiation. Crucially, ^{3}NQ* acts as an endogenous oxidant, driving efficient hydrogen abstraction from key organic classes without requiring external oxidants. Oxidation kinetics exhibit a striking hierarchy governed by bond dissociation energies and one-electron oxidation potentials: alkanes (10^4 $M^{-1}s^{-1}$) < oxygenated alkanes (10^5 $M^{-1}s^{-1}$) < phenols (10^6 $M^{-1}s^{-1}$). Radical intermediates (alkyl, alkoxyl, phenoxy) dehydrogenate into stable products (e.g., benzoquinone from phenol), while the self-photoconversion product OH–NQ regenerates a secondary triplet (^{3}OH–NQ*), amplifying oxidative cascades. This establishes ^{3}BrC* as the dominant sink for phenols in BrC-rich haze, particularly under acidic, O_2-limited conditions. Our findings provide kinetic and mechanistic benchmarks for integrating triplet-state chemistry into atmospheric models, advancing predictions of SOA formation in regions plagued by severe particulate pollution.

1. Introduction

Secondary organic aerosols (SOA), accounting for 25 %–30 % of $PM_{2.5}$ mass during China's severe haze episodes, are critically shaped by heterogeneous reactions of volatile organic compounds in atmospheric condensed phases (Huang et al., 2014; Zhang et al., 2015, 2022). While traditional models emphasize gas-phase oxidation, mounting evidence highlights multiphase processes, particularly aqueous-phase reactions in suspended microdroplets, as dominant drivers of SOA formation and aging (Felber et al., 2021; Griffith et al., 2013). However, persistent underestimations of SOA burdens in atmospheric models, especially during high-brown carbon (BrC) haze events in regions like East Asia, suggest missing chemical mechanisms (Zheng et al., 2015). Field observations report BrC concentrations in Asian hotspots ~10-fold higher than in Europe or North America (Jo et al., 2016; Xiong et al., 2022), yet the photochemical role of BrC in SOA amplification remains poorly constrained in models. These processes involve photooxidation and acid-catalyzed oxidation (e.g., driven by sulfuric/nitric acid), transforming dissolved organic compounds into oxidation products and oligomers (Ervens, 2015; Shrivastava et al., 2017; Smith et al., 2014). The unique aqueous environment in atmospheric condensed phases accelerates reaction kinetics, generating distinct free radicals and active intermediates while promoting hydrogen transfer and hydration, thereby establishing reaction networks diverging from gas-phase pathways (Dong et al., 2021; Kusaka et al., 2021). Despite this, mechanistic gaps persist in understanding how organic transformations in atmospheric liquid water govern aqueous SOA production, hindering accurate haze prediction.

Photosensitization, a process well-documented in aquatic chemistry, has emerged as a key pathway for the oxidation of organic compounds in atmospheric condensed phases, ultimately increasing the mass of SOA (George et al., 2015; Laskin et al., 2015; Li et al., 2019). For example, photosensitized reactions of aromatic carbonyls (e.g., 3,4-dimethoxybenzaldehyde) can convert phenols into aqueous SOA with

* Corresponding authors.
E-mail addresses: antc99@gdut.edu.cn (T. An), christian.george@ircelyon.univ-lyon1.fr (C. George).

https://doi.org/10.1016/j.jes.2025.10.037
Received 14 April 2025; Received in revised form 13 October 2025; Accepted 21 October 2025
Available online 25 October 2025

near-quantitative yields (Smith et al., 2014), suggesting that photosensitized processes may dominate over •OH oxidation in biomass-rich regions. Flow-tube experiments further demonstrate that atmospheric photosensitizers (e.g., humic acids, 4-benzoylbenzoic acid, and imidazole derivatives) induce radical chemistry in aerosols, promoting reactive organic uptake and substantial aerosol growth (Aregahegn et al., 2013; Monge et al., 2012; Rossignol et al., 2014). A critical class of such photosensitizers, aromatic carbonyls (e.g., acetophenones, benzaldehydes, and naphthoquinones), derived from anthropogenic and biogenic sources, is pervasive within chromophoric BrC (Kuang et al., 2023; Lee et al., 2014; Vione et al., 2006).

Given Asia's elevated BrC levels (Jo et al., 2016; Xiong et al., 2022), its potential role in SOA formation during haze events via triplet-state pathways warrants exploration. Central to BrC photochemistry is its excited triplet state (^{3}BrC*), formed via intersystem crossing from transient singlets under solar irradiation (Kaur et al., 2018; Smith et al., 2014). Despite its recognized oxidative potential, the mechanistic interplay between ^{3}BrC* and organics remains poorly defined, particularly regarding concurrent pathways (e.g., self-photoconversion vs. substrate oxidation) and structural substrate variations modulating reaction efficiency. Prior studies highlight ^{3}BrC*-mediated oxidation of specific compounds, biogenic alkenes (Li et al., 2016), phenols (Go et al., 2023; Kaur et al., 2019), and aromatic precursors (Go et al., 2022), and their contributions to SOA formation (Liang et al., 2024a). However, these works either focused on single substrate types or lacked resolution of mechanistic interdependencies (e.g., kinetic coupling between triplet self-transformation and substrate oxidation) and quantitative links to substrate properties. For instance, Li et al. (2016) observed diffusion-limited quenching of triplet imidazole-2-carboxaldehyde by isoprene but did not explore how C–H/O–H bond strengths govern oxidation kinetics across diverse organics. Similarly, Kaur et al. (2019) and Go et al. (2023) reported triplet-mediated phenol oxidation but did not dissect ^{3}BrC*'s dual roles in self-photoconversion (e.g., hydroxylation) and substrate oxidation, nor establish a hierarchical efficiency framework across compound classes.

To address these mechanistic gaps, we selected 1,4-naphthoquinone (NQ), a prevalent BrC photosensitizer in atmospheric aerosols (Kuang et al., 2023), as a model compound to investigate its triplet state (^{3}NQ*) in aqueous systems representing high-relative-humidity (RH) haze. Leveraging NQ's well-characterized photochemistry and high reactivity provides an ideal proxy for elucidating fundamental triplet-state processes in BrC-rich environments, although future work should extend to mixed organic-water phases to address full aerosol complexity. Three representative organic classes exhibiting distinct hydrogen-donating capacities were studied: phenols (dominant SOA precursors in biomass-rich haze) (Gilardoni et al., 2016), oxygenated alkanes (models for oxidized organics) (Shen et al., 2013), and alkanes (low-reactivity benchmarks) (Benish et al., 2020). This selection enables systematic evaluation of bond dissociation energy (BDE)-dependent ^{3}NQ* reactivity. Notably, ^{3}NQ* possesses a substantially higher one-electron reduction potential than other atmospheric photosensitizers (Liang et al., 2024b; McNeill et al., 2016), significantly enhancing its capacity for electron- and hydrogen-transfer reactions and establishing it as a potent endogenous oxidant. Three key questions drive this work: (i) how concurrent pathways of ^{3}NQ* decay, self-photoconversion to hydroxylated NQ (OH–NQ) versus substrate oxidation via hydrogen abstraction, compete under deoxygenated conditions; (ii) what hierarchical oxidation efficiency (phenols > oxygenated alkanes > alkanes) emerges across organic classes and how it correlates with C–H/O–H BDEs; (iii) what radical-mediated products form and by what mechanisms. These questions are addressed through integrated pulsed laser excitation coupled with transient absorption spectroscopy, atmospheric pressure chemical ionization high-resolution mass spectrometry (APCI-HRMS), and gas chromatography-mass spectrometry (GC–MS), establishing a mechanistic and kinetic framework to advance predictive modeling of BrC-driven SOA formation in pollution hotspots.

2. Materials and methods

2.1. Chemicals

All chemicals were used as purchased without further purification. All solutions were freshly prepared using ultrapure water (Elga Purelab Classic, 18.2 MΩ·cm). 1,4-naphthoquinone (NQ) solution was ultrasonically treated for 10 min to promote its dissolution. In addition, N_2 (99.999 %) was used in this study.

2.2. Pulsed laser excitation experiments

The transient absorption spectra of the excited NQ with/without organic reactants were measured using a pump-probe system combined with a classical laser flash excitation apparatus described earlier (Wang et al., 2020). The photolysis excitation source was the second harmonic (355 nm, pulse width ~7 ns) of a Nd:YAG laser (Surelite II 10, Continuum, USA) operated in the single-shot mode. During the experiments, the laser pulse energy was limited to 30 mJ per pulse (18 mJ/cm^2) to avoid the possible photolysis of NQ and possible interferences from products. The NQ solution was introduced in the flow cell of 0.45 mL by means of a peristaltic pump, with a flow of 1.6 mL/min for limiting the exposition of the introduced solution to 3–4 laser shots and maintaining its constant temperature. All solutions were ultrasonicated for 1 min before measurements to ensure complete dissolution and deoxygenated by N_2 bubbling (≥ 30 min) with continuous N_2 flow during experiments to eliminate O_2 interference. Solution pH was measured after N_2 saturation using a calibrated pH meter prior to laser irradiation experiments. For insoluble alkanes, solutions were ultrasonically premixed with NQ and magnetically agitated during measurements to maximize collision efficiency. It should be noted that the concentration of alkanes shown in this work can only be regarded as an equivalent concentration, which is calculated on the assumption that the alkanes and NQ aqueous solutions are fully and uniformly mixed. For construction of an absorption spectrum, measurements were repeated every 10–20 nm between 360 nm and 660 nm. For the kinetic measurements, the probe wavelengths for the transient absorption decay of NQ triplet state were 390 and 520 nm, two maxima in the triplet state absorption spectra. Typically, signals from 64 repeated pulses were averaged for each observation wavelength.

2.3. Analysis of products

For the APCI-HRMS analysis (HRMS-Orbitrap, Q Exactive, Thermo Scientific, Bremen, Germany), APCI spray current of −10.0 uA and +4.0 uA were applied for negative and positive ionization mode measurements, respectively. Additionally, the sheath gas flow rate was set to 40 arbitrary units (au) and the auxiliary gas flow rate to 10 au. A capillary temperature of 320 °C and a heater temperature of 350 °C were used. All measurements were performed using a resolution of 70,000 FWHM and the scanning range was set to *m/z* 50–750. Instrument controlling and data acquiring were performed using an Xcalibur workstation (Thermo Fisher Scientific, USA). All of the exact mass assignments to chemical formula were done considering carbon, hydrogen, oxygen as potential elements and with a mass accuracy below 5 ppm. For the GC–MS analysis, aqueous samples were analyzed via purge-and-trap gas chromatography-mass spectrometry (P&T-GC–MS; Agilent 7890B-5977B, USA) to enable direct analysis of volatile organic compounds in aqueous matrices. After pulsed laser excitation experiments, the reaction solutions were transferred undiluted into 50 mL airtight centrifuge tubes (filled to capacity) and introduced into the P&T system. The sample was purged with helium (40 mL/min, 10 min) to transfer volatiles onto a Tenax® sorbent trap, followed by thermal desorption (250 °C) into the P&T-GC–MS equipped with a HP-5MS capillary column (30 m × 250 μm × 0.25 μm). The GC operational parameters were as follows: initially 60 °C for 0 min, programmed to 161 °C at a rate of

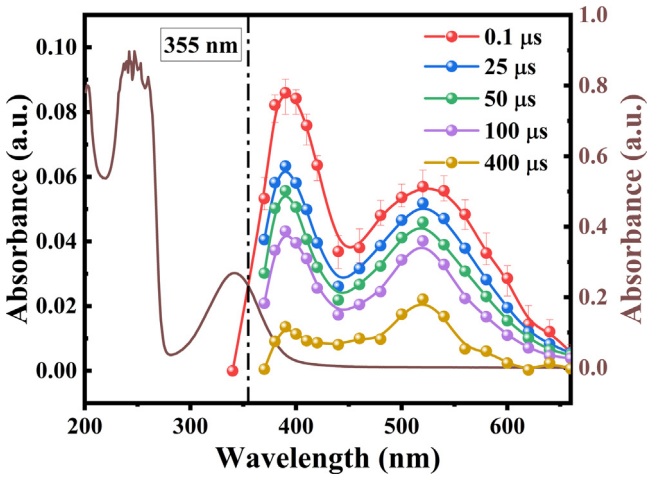

Fig. 1 – Absorption and transient absopriton spectra of 0.4 mM N_2-saturated 1,4-naphthoquinone (NQ) aqueous solution. The solid line (–) shows the UV–vis absorption spectra of solutions before the laser excitation (right Y-axis), and the transient absorption spectra (left Y-axis) were recorded at 0.1, 25, 50 and 100 μs after 355 nm laser flash photolysis.

3 °C/min, and finally to 280 °C at a rate of 10 °C/min and held for 1 min. The MS was operated in full scan mode with *m/z* of 50–450, while the temperature of the transfer line and ionizing energy were set at 230 °C and 70 eV. The carrier gas was ultra-high purity helium with flow rate of 1.0 mL/min. The qualitative identification of the intermediates was accomplished through comparing their mass spectra with the National Institute of Standards and Technology (NIST) database.

3. Results

3.1. Characteristics of the triplet state NQ

The UV–vis absorption spectrum of 0.4 mM N_2-saturated NQ aqueous solution (Fig. 1) exhibited strong absorption between 300 and 400 nm, confirming efficient excitation by 355 nm laser pulses. Laser flash photolysis of NQ in deoxygenated aqueous solutions allowed the identification of a rather long-lived transient species, attributed to NQ excited triplet state (^{3}NQ*). Fig. 1 shows recorded transient absorption spectra of N_2-saturated NQ solutions at different time intervals after the laser pulse, and the intense absorptions can be observed in the first 0.1 μs, characterized by two distinct peaks with the maximum around 390 and 520 nm respectively. The 390 nm peak intensity dominated over 520 nm, with both decaying non-uniformly over 25–400 μs. Incomplete return to baseline absorption (380–600 nm) suggested persistent light-absorbing photoproducts. Notably, this transient spectrum differs markedly from reports in acetonitrile, where only a single ^{3}NQ* peak at 365 nm is observed (Amada et al., 1995). This contrast implies solvent-dependent photophysics: the redshift to 390 nm in water likely arises from hydrogen bonding and/or nucleophilic interactions that alter ^{3}NQ* relaxation pathways. The persistent 520 nm band, absent in aprotic solvents, suggests a water-specific photochemical process generating secondary triplet species. While the 390 nm band is attributed to the triplet-triplet (T-T) transition of ^{3}NQ*, the origin of the 520 nm feature requires further mechanistic investigation, as discussed below.

Fig. 2**a** shows recorded transient absorption spectra of 0.4 mM N_2-saturated NQ aqueous solution before and after a single measurement cycle consisting of 64 consecutive laser pulses. Following irradiation, the transient absorption maximum at 390 nm diminished, while a notable increase occurred at 520 nm, suggesting self-quenching of ^{3}NQ* generates new products and facilitates the formation of a secondary triplet state at 520 nm. Decay kinetics monitored at 390 nm and 520 nm (Fig. 2**b and c**) followed single-exponential behavior. The pseudo-first-order rate constant (k_{obs}) obtained from the slope of a logarithmic plot of the transient signals over the 0–50 μs region are $k_{390,N_2} = 8.1 \times 10^3$ s^{-1} and $k_{520,N_2} = 3.7 \times 10^3$ s^{-1}, respectively. Corresponding lifetimes ($\tau = 1/k$) were calculated as $\tau_{390,N_2} = 123$ μs and $\tau_{520,N_2} = 270$ μs under deoxygenated conditions. These lifetimes align with reported ^{3}(n, π^*) configurations (10^{-4}–10^{-2} s) (Felber et al., 2021; Wardle, 2009), confirming both triplet states as ^{3}(n, π^*). When NQ solutions were exposed to air, the ^{3}NQ* lifetime shortened to $\tau_{390,Air} = 95$ μs due to partial O_2 quenching, while the 520 nm state remained unaffected ($\tau_{520,Air} = 253$ μs). The reduction in ^{3}NQ* lifetime (from 123 μs in N_2 to 95 μs in air) confirms partial O_2 quenching. However, this lifetime significantly exceeds the diffusion-controlled limit (<10 μs) expected for high-energy triplets at dissolved $[O_2] \approx 2.5 \times 10^{-4}$ M and typical $k_q(O_2) \geq 10^9$ $M^{-1}s^{-1}$ (Felber et al., 2021). This deviation arises because ultrafast nonradiative decay pathways (e.g., intersystem crossing) dominate ^{3}NQ* deactivation, kinetically outcompeting O_2 quenching despite thermodynamic favorability ($E_T \approx 241$ kJ/mol ≫ 94 kJ/mol threshold for $^1O_2$ formation) (McNeill et al., 2016). The calculated $k_q(O_2) \approx 9.6 \times 10^6$ $M^{-1}s^{-1}$ (derived from $\tau_{390,N_2} = 123$ μs, $\tau_{390,Air} = 95$ μs, and $[O_2] = 0.25$ mM) further confirms kinetic limitations. Conversely, the O_2-insensitivity of the 520 nm state ($\tau_{520,Air} \approx \tau_{520,N_2}$) directly reflects its triplet energy below the 94 kJ/mol threshold, rendering it inert to energy transfer (Felber et al., 2021; Moor et al., 2019).

Appendix A Fig. S1 demonstrates that increasing NQ concentration (≤ 0.5 mM) enhances transient absorption at 390 nm and 520 nm, indicating that within a particular concentration range, an increase in NQ content leads to a corresponding rise in the generation of 3NQ*. Self-quenching constants (k_{sq}) and intrinsic lifetimes (τ_0) were derived via Stern-Volmer analysis (Eq. (1)), as shown in Fig. 2d:

$$k_{obs} = 1/\tau_0 + k_{sq} \times [NQ] \quad (1)$$

In N_2-saturated aqueous solution, k_{sq} of ^{3}NQ* (390 nm) and the 520 nm state were estimated to be 5.6×10^4 and 1.7×10^4 $M^{-1}s^{-1}$, respectively, with their τ_0 being 123 and 270 μs, respectively.

The distinct O_2 reactivity and self-quenching kinetics of ^{3}NQ* (390 nm) versus the 520 nm state confirm their assignment to distinct photosensitizers. To identify the 520 nm species, post-irradiated NQ was analyzed by direct APCI-HRMS (highly sensitive to both polar and non-polar compounds), revealing a prominent product at *m/z* 173.02442 ± 0.00001 (negative ionization mode), corresponding to a neutral $C_{10}H_6O_3$ species (**Appendix A Fig. S2a**). Prior studies attribute this to hydroxylated NQ derivatives (5-/7-OH–NQ), formed via triplet-state heterolytic water addition involving H-atom migration and redox processes (Brahmia et al., 2003). kinetic analysis establishes water addition as the primary pathway for ^{3}NQ* decay. The self-quenching constant for ^{3}NQ* ($k_{sq} = 5.6 \times 10^4$ $M^{-1}s^{-1}$; Fig. 2**d**) yields an effective rate of only 22.4 s^{-1} at [NQ] = 0.4 mM. In contrast, the water addition rate constant ($k_{add} \approx 4 \times 10^4$ $M^{-1}s^{-1}$) dominates due to the high $[H_2O]$ (55.6 M), resulting in an effective rate (k_{add} $[H_2O]$) of ~2.2×10^6 s^{-1} (Brahmia et al., 2003). This >10^4-fold rate difference confirms OH–NQ as the principal photoproduct, consistent with the absence of dimeric species in HRMS controls. Critically, APCI-HRMS detected only OH–NQ in both N_2-saturated and air-exposed systems, with no signals for oxygenated dimers, peroxides, or other potential chromophores derived from O_2 involvement (**Appendix A Fig. S2**). This confirms O_2 does not significantly alter the primary photoproduct identity or generate new light-absorbing species under our experimental conditions. The water addition pathway also dominates over O_2 quenching (effective rate ~2.4×10^3 s^{-1} at $[O_2] = 0.25$ mM), ensuring OH–NQ formation irrespective of O_2. Spectroscopic (distinct peaks, differential O_2 sensitivity), kinetic (lifetimes, self-quenching constants), and mass-spectral identification (exclusive detection of OH–NQ) evidence collectively support the coexistence of ^{3}NQ* (390 nm) and the secondary triplet state of its photoproduct, ^{3}OH–NQ* (520 nm), in photoexcited aqueous NQ. While minor contributions to the 520 nm band from other species cannot be absolutely excluded, its O_2 insensitivity, correlation with OH–NQ for-

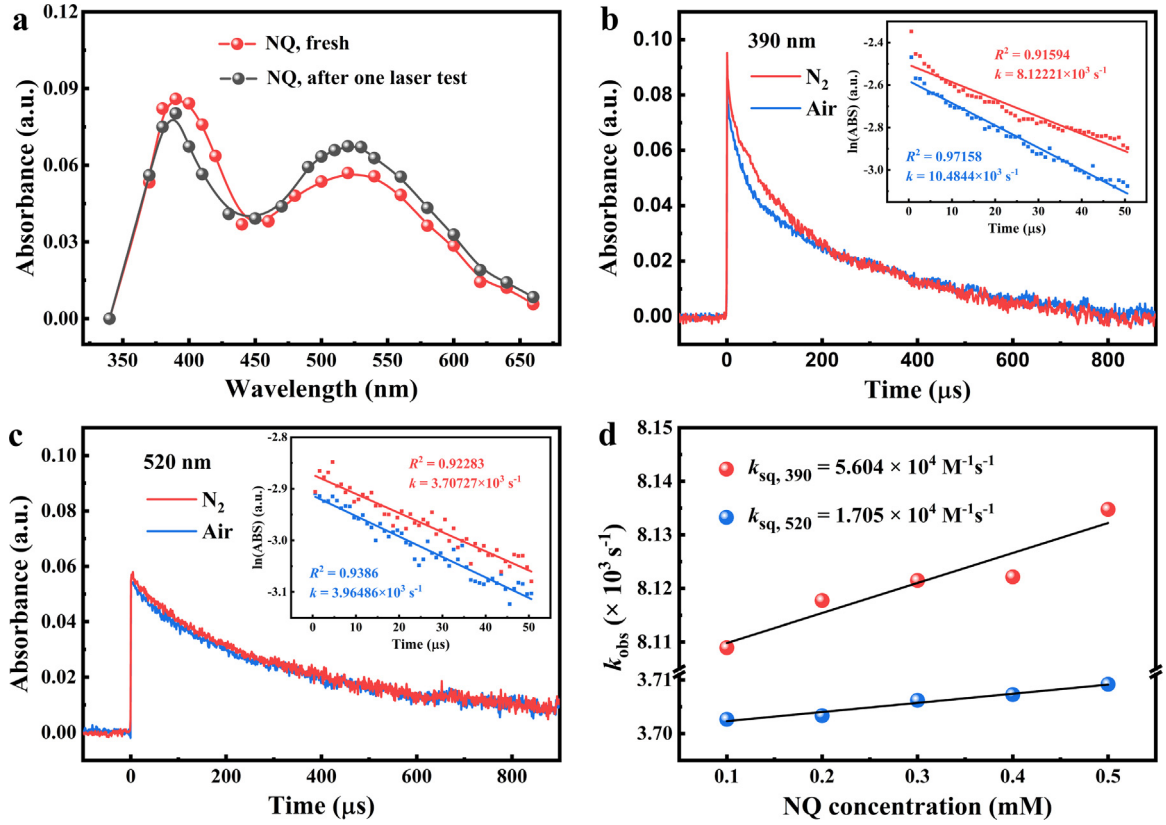

Fig. 2 – (a) Transient absorption spectra recorded at 0.1 μs after 355 nm laser flash photolysis of 0.4 mM N_2-saturated NQ aqueous solution before and after a single measurement cycle consisting of 64 consecutive laser pulses; (b, c) transient absorption decay obtained at 390 nm and 520 nm of NQ triplet state in 0.4 mM N_2-saturated or air-exposed NQ aqueous solution, with the corresponding log plot of a transient absorption decay (insert); (d) Stern-Volmer plots of the observed quenching first-order rate coefficients k_{obs} as a function of NQ concentration obtained at 390 and 520 nm.

mation, and the absence of alternative chromophoric products provide robust assignment to ^{3}OH–NQ*. Given the higher reactivity of ^{3}NQ* compared to ^{3}OH–NQ*, subsequent substrate oxidation kinetics focused solely on the 390 nm band.

3.2. Reactivity of 3NQ* with organic compounds

Fig. 3**a-c** show recorded transient absorption spectra of NQ with different concentrations of cyclohexane, ethanol and phenol, respectively. Since cyclohexane is insoluble in water, a magnetic stirrer was used to ensure adequate contact between cyclohexane and NQ throughout the pulsed laser excitation experiment. Notably, the transient absorption intensity of ^{3}NQ* (390 nm) increased with organics concentration, following the hierarchy: cyclohexane < ethanol < phenol. This intensity hierarchy contrasts with minor UV absorbance changes at 355 nm (phenol: +0.0098 < ethanol: +0.0109 < cyclohexane: +0.0117; **Appendix A Figs. S3-S5**). As initial NQ concentration (0.4 mM) was rigorously controlled and organics contributed negligibly to absorbance (ΔA ≤ 0.0004, **Appendix A Fig. S6**), these UV variations reflect solvent effects on NQ's absorption profile, and confirm the transient hierarchy is independent of excitation-wavelength absorbance. The observed transient intensity gradient arises from distinct mechanisms: ethanol's higher polarity enhances molecular collision efficiency relative to hydrophobic cyclohexane, whereas phenol dominance stems from protonation-driven photophysics. For phenol, the absorption peak blue-shifted to 380 nm at concentrations >1.0 mM, concurrent with pH decrease from 6.0 to 5.0 (Fig. 3**c** and **Appendix A Fig. S7**). This acidification (pH 5.0) approaches the pK_a of ground-state NQ (~4.2) (Rath et al., 1996), facilitating partial protonation to form mono-ionic NQ (NQH^+) with enhanced hydrophilicity. Protonation enhances the electron-deficient character of NQ, increasing its electrophilicity and triplet-state stability, while intermolecular hydrogen bonding (C=O·H–O) between NQH^+ and phenol selectively stabilizes the ^{3}(n, π^*) configuration of ^{3}NQ* (Rath et al., 1996). This dual effect: (i) raises the excited-state energy, widening the ground-to-excited-state gap from 3.18 eV (390 nm) to 3.26 eV (380 nm) (Amada et al., 1995; Song et al., 2013); (ii) enhances charge separation efficiency (Song et al., 2013); and (iii) boosts intersystem crossing in NQH^+ (Yang et al., 2021). While acidification alone (via H_2 SO_4) non-specifically increases both 390 nm (^{3}NQ*) and 520 nm (^{3}OH–NQ*) bands due to protonation-enhanced triplet yields (**Appendix A Fig. S8**), the phenol-specific H-bonding synergizes with protonation to preferentially amplify the ^{3}NQ* absorption at 390 nm (Fig. 3**c**). This occurs because the 520-nm band (^{3}OH–NQ*, from nucleophilic H_2O addition to ^{3}NQ*) is less responsive to H-bonding with phenol.

The transient absorption spectra of NQ with cyclohexane, ethanol, and phenol (recorded at 0.1–400 μs post-excitation) revealed uniform absorbance decay without new spectral bands (**Appendix A Fig. S9a-c**). The triplet-triplet absorption decay of ^{3}NQ* at 390 nm followed mono-exponential kinetics (**Appendix A Fig. S9d**), enabling determination of quenching rate coefficients (k_q) via Stern-Volmer analysis (Fig. 3**d**). The k_q values increased by one order of magnitude for ethanol relative to cyclohexane, and by another order for phenol relative to ethanol: 8.0 × 10^4, 1.2 × 10^5 and 4.8 × 10^6 $M^{-1}s^{-1}$, respectively. In parallel, the corresponding intrinsic lifetimes (τ_0) exhibited a progressive reduction, decreasing from 134.6 μs in cyclohexane, to 126.4 μs in ethanol, and finally to 123.0 μs in phenol. Notably, the ethanol-derived k_q (1.2 × 10^5 $M^{-1}s^{-1}$) aligned with the reported value for hydrogen abstraction by quinone triplets from alcohols (about 10^5 $M^{-1}s^{-1}$) (Harada et al., 2005), confirming our experimental reliability. The observed hierarchy in oxidation efficiency: alkanes <

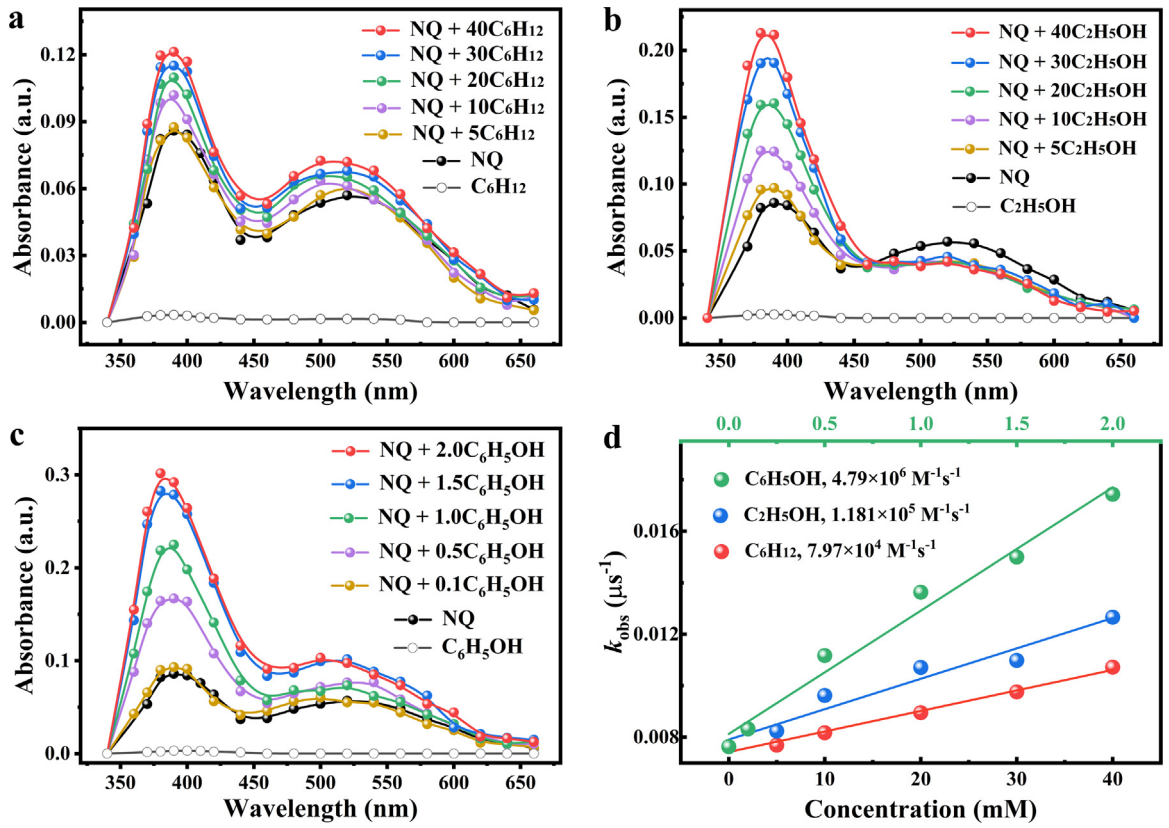

Fig. 3 – (a-c) Transient absorption spectra recorded at 0.1 μs after 355 nm laser flash photolysis of 0.4 mM N_2-saturated NQ aqueous solution with different concentrations of cyclohexane (equivalent concentration of 5, 10, 20, 30 and 40 mM), ethanol (5, 10, 20, 30 and 40 mM) and phenol (0.1, 0.5, 1.0, 1.5 and 2.0 mM); (d) Stern-Volmer plots of the observed quenching first-order rate coefficients k_{obs} as a function of cyclohexane, ethanol and phenol concentration obtained at 390 nm.

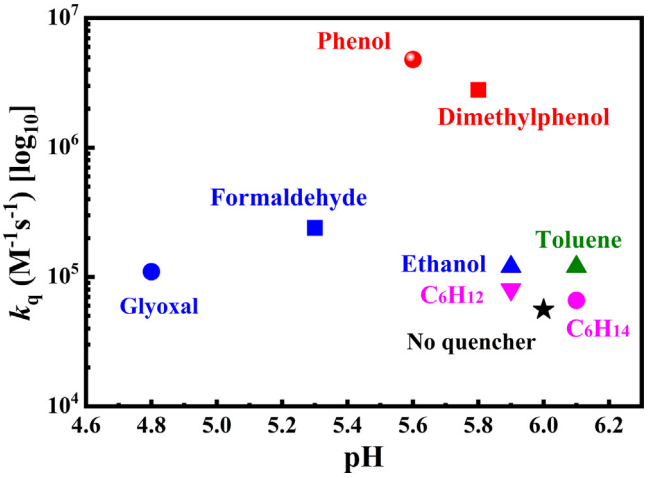

Fig. 4 – The quenching rates of $^3NQ^*$ in the absence and presence of organic compounds obtained at 390 nm. It should be noted that pH here is the pH of the solution itself without any adjusting, and values given in Appendix A Table S1.

oxygenated alkanes < phenols, correlates with the hydrogen/electron-donating capacities of these compounds, governed by two key physicochemical parameters: (i) Bond dissociation energies (BDEs) for the weakest C–H/O–H bonds: 96 kcal/mol (cyclohexane C–H) (Liu et al., 2022), 93 kcal/mol (ethanol α-C–H) (Alfassi et al., 1972; Oguri et al., 2014), and 87 kcal/mol (phenol O–H) (Mulder et al., 2005). Lower BDEs facilitate hydrogen-atom transfer (HAT), explaining phenol's two-order-of-magnitude higher k_q than cyclohexane (Fig. 4). (ii) One-electron oxidation potentials (OP): Phenols exhibit lower OPs than aliphatic compounds, enhancing their susceptibility to oxidation via proton-coupled electron transfer (PCET) (Kaur et al., 2019; McNeill et al., 2016). This gradient suggests mechanistic divergence: HAT dominates for aliphatic substrates (alkanes/oxygenated alkanes), while PCET prevails for phenols due to their lower OP and BDE (Kaur et al., 2019; McNeill et al., 2016). The role of OP is further evidenced by correlations between k_q and substrate OP across diverse organics. For example, Kaur et al. (R. Kaur et al., 2019) reported OP-dependence (R^2 = 0.58) for alkene reactions with triplet benzophenone, and McNeill et al. (2016) emphasized OP as a key descriptor for triplet-mediated oxidations. Recent compilations by Liang et al. (2024a) corroborate this hierarchy, showing that phenolic compounds with lower OP exhibit higher k_q (e.g., phenol: 2.9×10^8 $M^{-1}s^{-1}$) than oxygenated aliphatics (e.g., HCOOH: 2.0×10^5 $M^{-1}s^{-1}$) or alkanes/organic acids (e.g., succinate: 9.2×10^4 $M^{-1}s^{-1}$). This kinetic trend underscores OP as a complementary predictor to BDE for hydrogen/electron-donating capacity, particularly for substrates where PCET mechanisms are accessible (Dalton et al., 2025; McNeill et al., 2016).

3.3. Product formation and mechanism

Product identification from $^3NQ^*$-mediated organic compounds oxidation required complementary APCI-HRMS and GC–MS analyses, leveraging their respective strengths: APCI-HRMS for molecular formulas of non-volatile polar species (supporting speculated identities) and GC–MS for structural identification of low-molecular-weight volatiles via library matching (Table 1). Based on molecular formulas, hydroxylated NQ (OH–NQ; m/z 173.02442 $C_{10}H_6O_3$) is speculated as a universal byproduct across all reactions, reflecting competitive quenching between organic compounds and water for $^3NQ^*$. Phenol oxidation generated products assigned as benzoquinone (m/z 108.02168, $C_6H_4O_2$), hydro-

Table 1 – Molecular formulas and speculated identities of products detected by APCI-HRMS and GC–MS for NQ reactions in deoxygenated aqueous solutions.

m/z	Formula	NQ	NQ + cyclohexane	NQ + ethanol	NQ + phenol
(-) APCI-HRMS					
173.02442	$C_{10}H_6O_3$	●	●	●	●
108.02168	$C_6H_4O_2$				●
109.02946	$C_6H_6O_2$				●
217.05043	$C_{12}H_{10}O_4$				●
GC–MS					
82.0	C_6H_{10}		●		
44.1	C_2H_4O			●	

Note: APCI-HRMS provides molecular formulas (exact masses) that support speculated compound identities; structural assignments are not definitively confirmed by this technique alone. GC–MS identifications are based on library matching (NIST).

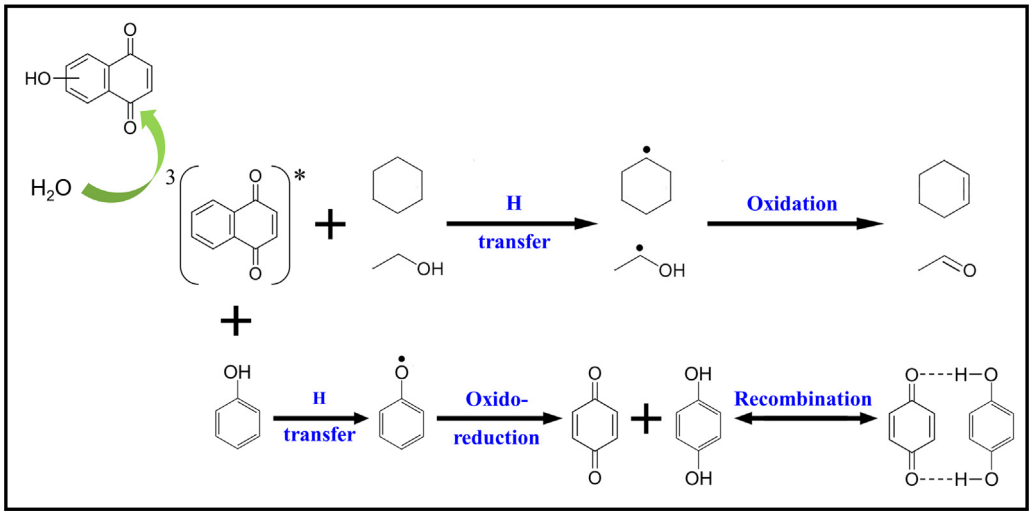

Fig. 5 – Potential formation mechanisms of organic compounds oxidation induced by $^3NQ^*$.

quinone (*m/z* 109.02946, $C_6H_6O_2$), and quinhydrone (*m/z* 217.05043, $C_{12}H_{10}O_4$) based on exact masses and prior literature, though structural confirmation requires further validation, while ethanol and cyclohexane yielded acetaldehyde (C_2H_4O) and cyclohexene (C_6H_{10}), respectively. Notably, these products formed without external oxidants, consistent with $^3NQ^*$'s intrinsic hydrogen abstraction capability. Mechanistically, oxidation proceeds via direct hydrogen transfer or sequential electron-proton transfer, generating phenoxy, alkoxyl, and alkyl radicals as key intermediates.

The proposed reaction mechanism (Fig. 5) involves hydrogen abstraction from organic compounds by photoexcited $^3NQ^*$, initiating oxidation cascades. For cyclohexane and ethanol, direct hydrogen transfer to $^3NQ^*$ generates alkyl or alkoxyl radicals, which dehydrogenate into stable products (cyclohexene or acetaldehyde). In contrast, phenol reacts *via* formation of a charge-transfer exciplex through coulombic interactions or hydrogen bonding with $^3NQ^*$, followed by sequential electron-proton transfer to yield phenoxy radicals (Lathioor et al., 2006; Leigh et al., 1996; Remke et al., 2022]. These radicals undergo redox reactions in deoxygenated aqueous media, producing benzoquinone and hydroquinone. Subsequent recombination of these products forms quinhydrone, driven by (1) electron-rich hydroquinone coordinating with electron-deficient benzoquinone and (2) hydrogen bonding between hydroquinone's hydroxyl group and benzoquinone's carbonyl moiety. Concurrently, $^3NQ^*$ undergoes self-photoconversion to OH–NQ, which forms a secondary triplet species, amplifying oxidative cycles in the aqueous phase.

4. Conclusions

Our systematic investigation reveals that pulsed laser excitation of deoxygenated aqueous NQ, a key BrC proxy, generates two reactive triplet states ($^3NQ^*$ and $^3OH–NQ^*$) with $^3(n, \pi^*)$ configurations. Crit-

ically, $^3NQ^*$ oxidizes organic compounds via hydrogen abstraction with a marked efficiency hierarchy: alkanes (10^4 $M^{-1}s^{-1}$) < oxygenated alkanes (10^5 $M^{-1}s^{-1}$) < phenols (10^6 $M^{-1}s^{-1}$). This gradient is governed by bond dissociation energies (C–H/O–H) and one-electron oxidation potentials, which collectively modulate hydrogen/electron-donating capacities. The process operates independently of external oxidants (e.g., O_2), establishing $^3NQ^*$ as a dominant sink for phenols in BrC-rich environments, with efficiency rivaling •OH and $^1O_2$ under acidic conditions that enhance protonation and intermolecular H-bonding.

These mechanistic insights are critically relevant to severe haze episodes (e.g., in East Asia), where: (i) high relative humidity (>80 %) partitions water-soluble precursors (phenols, oxygenated alkanes) into aerosol aqueous phases, creating optimal media for triplet-driven chemistry; (ii) despite light attenuation by particulate matter, BrC's efficient photon harvesting sustains triplet generation, and the kinetic hierarchy persists due to linear scaling with actinic flux; (iii) low aerosol pH (about 4–5) synergistically enhances triplet yields via BrC protonation while promoting phenolic reactivity; (iv) the O_2 independence of $^3BrC^*$ enables persistent oxidation in O_2-depleted environments. Product analysis confirms dual pathways, substrate oxidation and $^3NQ^*$ self-conversion to OH–NQ, that collectively amplify oxidative cascades. Collectively, this work provides essential kinetic and mechanistic benchmarks for integrating triplet-state chemistry into atmospheric models, advancing predictions of SOA formation in regions plagued by severe particulate pollution.

CRediT authorship contribution statement

Jiejing Kong: Writing – review & editing, Writing – original draft, Investigation, Data curation. **Mingzhu He:** Investigation. **Jintao Liu:** Investigation. **Xinke Wang:** Investigation. **Taicheng An:** Writing – review & editing, Writing – original draft, Validation, Supervision, Resources, Project administration, Formal analysis, Conceptualization. **Christian George:** Writing – review & editing, Writing – original draft, Supervision, Resources, Project administration, Methodology, Formal analysis, Conceptualization.

Declaration of competing interest

The authors declare that they have no known competing financial interests or personal relationships that could have appeared to influence the work reported in this paper.

Acknowledgments

This work was supported by National Natural Science Foundation of China (Nos. 42020104001, 42377099 and 42007315), the European Research Council under the Horizon 2020 research and innovation programme/ERC Grant Agreement 101052601-SOFA, Guangdong Basic and Applied Basic Research Foundation (Nos. 2024A1515030144 and 2022A1515011465), and Guangzhou Science and technology project (No. 2024A04J0596).

Appendix A Supplementary data

Supplementary material associated with this article can be found in the online version at doi:10.1016/j.jes.2025.10.037.

References

Alfassi, Z., Golden, D., 1972. Bond dissociation energy of the carbon-hydrogen bond in ethanol. Kinetic study of the reaction iodine+ ethanol. J. Phys. Chem. 76 (23), 3314–3319.

Amada, I., Yamaji, M., Sase, M., Shizuka, H., 1995. Laser flash photolysis studies on hydrogen atom abstraction from phenol by triplet naphthoquinones in acetonitrile. J. Chem. Soc. Faraday Trans. 91 (17), 2751–2759.

Aregahegn, K., Nozière, B., George, C., 2013. Organic aerosol formation photo-enhanced by the formation of secondary photosensitizers in aerosols. Faraday Discuss. 165, 123–134.

Benish, S., He, H., Ren, X., Roberts, S., Salawitch, R., Li, Z., et al., 2020. Measurement report: aircraft observations of ozone, nitrogen oxides, and volatile organic compounds over Hebei Province, China. Atmos. Chem. Phys. 20 (23), 14523–14545.

Brahmia, O., Richard, C., 2003. Phototransformation of 1,4-naphthoquinone in aqueous solution. Photochem. Photobiol. Sci. 2 (10), 1038–1043.

Dalton, E., Wang, X., Wappes, S., Petersen-Sonn, E., Hagan, S., George, C., et al., 2025. Photosensitizers regulate nitrate photoproduct yields in bulk aqueous matrices. Environ. Sci. Technol. 59 (12), 6142–6154.

Dong, P., Chen, Z., Qin, X., Gong, Y., 2021. Water significantly changes the ring-cleavage process during aqueous photooxidation of toluene. Environ. Sci. Technol. 55 (24), 16316–16325.

Ervens, B., 2015. Modeling the processing of aerosol and trace gases in clouds and fogs. Chem. Rev. 115 (10), 4157–4198.

Felber, T., Schaefer, T., He, L., Herrmann, H., 2021. Aromatic carbonyl and nitro compounds as photosensitizers and their photophysical properties in the tropospheric aqueous phase. J. Phys. Chem. A 125 (23), 5078–5095.

George, C., Ammann, M., D'Anna, B., Donaldson, D., Nizkorodov, S., 2015. Heterogeneous photochemistry in the atmosphere. Chem. Rev. 115 (10), 4218–4258.

Gilardoni, S., Massoli, P., Paglione, M., Giulianelli, L., Carbone, C., Rinaldi, M., et al., 2016. Direct observation of aqueous secondary organic aerosol from biomass-burning emissions. PNAS 113 (36), 10013–10018.

Go, B., Li, Y., Huang, D., Wang, Y., Chan, C., 2023. Comparison of aqueous secondary organic aerosol (aqSOA) product distributions from guaiacol oxidation by non-phenolic and phenolic methoxybenzaldehydes as photosensitizers in the absence and presence of ammonium nitrate. Atmos. Chem. Phys. 23 (4), 2859–2875.

Go, B., Lyu, Y., Ji, Y., Li, Y., Huang, D., Li, X., et al., 2022. Aqueous secondary organic aerosol formation from the direct photosensitized oxidation of vanillin in the absence and presence of ammonium nitrate. Atmos. Chem. Phys. 22 (1), 273–293.

Griffith, E.C., Carpenter, B.K., Shoemaker, R.K., 2013. Vaida, V. Photochemistry of aqueous pyruvic acid. PNAS 110 (29), 11714–11719.

Harada, Y., Suzuki, T., Ichimura, T., 2005. III-F photophysics and photochemistry of aromatic molecules in the condensed phase. J. Photochem. Photobiol. A 170, 161–167.

Huang, R., Zhang, Y., Bozzetti, C., Ho, K., Cao, J., Han, Y., et al., 2014. High secondary aerosol contribution to particulate pollution during haze events in China. Nature 514 (7521), 218–222.

Jo, D., Park, R., Lee, S., Kim, S., Zhang, X., 2016. A global simulation of brown carbon: implications for photochemistry and direct radiative effect. Atmos. Chem. Phys. 16 (5), 3413–3432.

Kaur, R., Anastasio, C., 2018. First measurements of organic triplet excited states in atmospheric waters. Environ. Sci. Technol. 52 (9), 5218–5226.

Kaur, R., Hudson, B., Draper, J., Tantillo, D., Anastasio, C., 2019. Aqueous reactions of organic triplet excited states with atmospheric alkenes. Atmos. Chem. Phys. 19 (7), 5021–5032.

Kuang, Y., Shang, J., Sheng, M., Shi, X., Zhu, J., Qiu, X., 2023. Molecular composition of Beijing PM2.5 brown carbon revealed by an untargeted approach based on gas chromatography and time-of-flight mass spectrometry. Environ. Sci. Technol. 57 (2), 909–919.

Kusaka, R., Nihonyanagi, S., Tahara, T., et al., 2021. The photochemical reaction of phenol becomes ultrafast at the air-water interface. Nat. Chem. 13 (4), 306–311.

Laskin, A., Laskin, J., Nizkorodov, S., 2015. Chemistry of atmospheric brown carbon. Chem. Rev. 115 (10), 4335–4382.

Lathioor, E., Leigh, W., 2006. Bimolecular hydrogen abstraction from phenols by aromatic ketone triplets. Photochem. Photobiol. 82 (1), 291–300.

Lee, H., Aiona, P., Laskin, A., Laskin, J., Nizkorodov, S., 2014. Effect of solar radiation on the optical properties and molecular composition of laboratory proxies of atmospheric brown carbon. Environ. Sci. Technol. 48 (17), 10217–10226.

Leigh, W., Lathioor, E., St. Pierre, M., 1996. Photoinduced hydrogen abstraction from phenols by aromatic ketones. A new mechanism for hydrogen abstraction by carbonyl n, π^* and π, π^* triplets. J. Am. Chem. Soc. 118 (49), 12339–12348.

Li, S., Jiang, X., Roveretto, M., George, C., Liu, L., Jiang, W., et al., 2019. Photochemical aging of atmospherically reactive organic compounds involving brown carbon at the air-aqueous interface. Atmos. Chem. Phys. 19 (15), 9887–9902.

Li, W., Li, X., Jockusch, S., Wang, H., Xu, B., Wu, Y., et al., 2016. Photoactivated production of secondary organic species from isoprene in aqueous systems. J. Phys. Chem. A 120 (45), 9042–9048.

Liang, Z., Li, Y., Go, B., Chan, C., 2024a. Complexities of photosensitization in atmospheric particles. ACS ES&T Air 1 (11), 1333–1351.

Liang, Z., Zhou, L., Chang, Y., Qin, Y., Chan, C., 2024b. Biomass-burning organic aerosols as a pool of atmospheric reactive triplets to drive multiphase sulfate formation. PNAS 121 (51), e2416803121.

Liu, L., Chen, S., Xu, H., Zhu, Q., Ren, H., 2022. Effect of alkyl substituent for cyclohexane on pyrolysis towards sooting tendency from theoretical principle. J. Anal. Appl. Pyrol. 161, 105386.

McNeill, K., Canonica, S., 2016. Triplet state dissolved organic matter in aquatic photochemistry: reaction mechanisms, substrate scope, and photophysical properties. Environ. Sci-Proc. Imp. 18 (11), 1381–1399.

Monge, M., Rosenørn, T., Favez, O., Müller, M., Adler, G., Abo Riziq, A., et al., 2012. Alternative pathway for atmospheric particles growth. PNAS 109 (18), 6840–6844.

Moor, K., Schmitt, M., Erickson, P., McNeill, K., 2019. Sorbic acid as a triplet probe: triplet energy and reactivity with triplet-state dissolved organic matter via $^1O_2$ phosphorescence. Environ. Sci. Technol. 53 (14), 8078–8086.

Mulder, P., Korth, H., Pratt, D., DiLabio, G., Valgimigli, L., Pedulli, G., et al., 2005. Critical re-evaluation of the O–H bond dissociation enthalpy in phenol. J. Phys. Chem. A 109 (11), 2647–2655.

Oguri, T., Shimamura, K., Shibuta, Y., Shimojo, F., Yamaguchi, S., 2014. Bond dissociation mechanism of ethanol during carbon nanotube synthesis via alcohol catalytic

CVD technique: ab initio molecular dynamics simulation. Chem. Phys. Lett. 595-596, 185–191.
Rath, M., Pal, H., Mukherjee, T., 1996. One-electron transfer reactions of some hydroxynaphthoquinones solvent and substitution effect as studied by pulse radiolysis. J . Chem. Soc. Faraday Trans. 92 (11), 1891–1897.
Remke, S., Bürgin, T., Ludvíková, L., Heger, D., Wenger, O., von Gunten, U., et al., 2022. Photochemical oxidation of phenols and anilines mediated by phenoxyl radicals in aqueous solution. Water Res. 213, 118095.
Rossignol, S., Aregahegn, K., Tinel, L., Fine, L., Nozière, B., George, C., 2014. Glyoxal induced atmospheric photosensitized chemistry leading to organic aerosol growth. Environ. Sci. Technol. 48 (6), 3218–3227.
Shen, X., Zhao, Y., Chen, Z., Huang, D., 2013. Heterogeneous reactions of volatile organic compounds in the atmosphere. Atmos. Environ. 68, 297–314.
Shrivastava, M., Cappa, C., Fan, J., Goldstein, A., Guenther, A., Jimenez, J., et al., 2017. Recent advances in understanding secondary organic aerosol: implications for global climate forcing. Rev. Geophys. 55 (2), 509–559.
Smith, J., Sio, V., Yu, L., Zhang, Q., Anastasio, C., 2014. Secondary organic aerosol production from aqueous reactions of atmospheric phenols with an organic triplet excited state. Environ. Sci. Technol. 48 (2), 1049.
Song, P., Ma, F., 2013. Intermolecular hydrogen-bonding effects on photophysics and photochemistry. Int. Rev. Phys. Chem. 32 (4), 589–609.
Vione, D., Maurino, V., Minero, C., Pelizzetti, E., Harrison, M., Olariu, R., et al., 2006. Photochemical reactions in the tropospheric aqueous phase and on particulate matter. Chem. Soc. Rev. 35 (5), 441–453.
Wang, X., Gemayel, R., Hayeck, N., Perrier, S., Charbonnel, N., Xu, C., et al., 2020. Atmospheric photosensitization: a new pathway for sulfate formation. Environ. Sci. Technol. 54 (6), 3114–3120.
Wardle, B., 2009. Principles and Applications of Photochemistry. John Wiley & Sons.
Xiong, R., Li, J., Zhang, Y., Zhang, L., Jiang, K., Zheng, H., et al., 2022. Global brown carbon emissions from combustion sources. Environ. Sci. Ecotechnol. 12, 100201.
Yang, J., Acharjya, A., Ye, M., Rabeah, J., Li, S., Kochovski, Z., et al., 2021. Protonated imine-linked covalent organic frameworks for photocatalytic hydrogen evolution. Angew. Chem. Int. Ed. 60 (36), 19797–19803.
Zhang, R., Wang, G., Guo, S., Zamora, M.L., Ying, Q., Lin, Y., et al., 2015. Formation of urban fine particulate matter. Chem. Rev. 115 (10), 3803–3855.
Zhang, R., Gen, M., Liang, Z., Li, Y., Chan, C., 2022. Photochemical reactions of glyoxal during particulate ammonium nitrate photolysis: brown carbon formation, enhanced glyoxal decay, and organic phase formation. Environ. Sci. Technol. 56 (3), 1605–1614.
Zheng, B., Zhang, Q., Zhang, Y., He, K.B., Wang, K., Zheng, G., et al., 2015. Heterogeneous chemistry: a mechanism missing in current models to explain secondary inorganic aerosol formation during the January 2013 haze episode in North China. Atmos. Chem. Phys. 15 (4), 2031–2049.